Research Square

Preprints are preliminary reports that have not undergone peer review.
They should not be considered conclusive, used to inform clinical practice,
or referenced by the media as validated information.

The cardiovascular endophenotype of major depressive disorder: A right-heart-predominant remodelling pattern

Dengnan Zhang
Zhejiang University
Zhengyao Ding
Zhejiang University
Kewen Wang
Zhejiang University
Yujian Hu
Zhejiang University
Kemeng Zhang
Massachusetts Institute of Technology
Yue Wang
Zhejiang University
Yiheng Mao
Zhejiang University
Ziyu Li
Zhejiang University
Fan Yi
Zhejiang University
Mor Peleg
University of Haifa
Judith Somekh
University of Haifa
Zhentao Tang
Huawei Technologies (China)
MingXuan Yuan
Huawei Technologies (China)
Junhang Zhang
Hangzhou Seventh Peoples Hospital
Hongkun Zhang
Zhejiang University
Fei Wu

Zhejiang University

Hongjing Mao

Hangzhou Seventh Peoples Hospital

Ting Chen

Zhejiang University

Zhengxing Huang

zhengxinghuang@zju.edu.cn

Zhejiang University

Research Article

Keywords: Major depressive disorder, cardiovascular magnetic resonance, cardiac remodelling, right heart, cardiovascular disease

Posted Date: November 25th, 2026

DOI: https://doi.org/10.21203/rs.3.rs-11521203/v1

License: This work is licensed under a Creative Commons Attribution 4.0 International License. Read Full License

Additional Declarations: No competing interests reported.

The cardiovascular endophenotype of major depressive disorder: A right-heart-predominant remodelling pattern

Dengnan Zhang[1,*], Zhengyao Ding[2,*], Kewen Wang[3], Yujian Hu[4], Kemeng Zhang[5], Yue Wang[6], Yiheng Mao[2], Ziyu Li[2], Fan Yi[2], Mor Peleg[7], Judith Somekh[7], Zhentao Tang[8], Mingxuan Yuan[8], Junhang Zhang[9], Hongkun Zhang[4], Fei Wu[1,2], Hongjing Mao[9,#], Ting Chen[10,#], Zhengxing Huang[1,2,#]

[1] College of Artificial Intelligence, Zhejiang University, Hangzhou, Zhejiang Province, China
[2] College of Computer Science and Technology, Zhejiang University, Hangzhou, China
[3] College of Pharmaceutical Sciences, Zhejiang University, Hangzhou, China
[4] Department of Vascular Surgery, The First Affiliated Hospital, Zhejiang University School of Medicine, Hangzhou, China
[5] Sloan School of Management, Massachusetts Institute of Technology, Cambridge, Massachusetts, US
[6] Zhejiang University School of Medicine, Hangzhou, China
[7] Department of Information Systems, University of Haifa, Haifa, Israel
[8] Noah's Ark Lab, Huawei, Beijing, China
[9] Affiliated Mental Health Center & Hangzhou Seventh People's Hospital, Zhejiang University School of Medicine, Hangzhou, Zhejiang, China
[10] Department of Cardiology, The First Affiliated Hospital, Zhejiang University School of Medicine, Hangzhou, Zhejiang Province, China

[*] These authors contributed equally to this work.
[#] Corresponding authors. Address correspondence to: Hongjing Mao; 13777861972@163.com, Ting Chen; ct010151452@zju.edu.cn, and Zhengxing Huang; zhengxinghuang@zju.edu.cn.

Abstract

Background Major depressive disorder (MDD) is associated with increased cardiovascular morbidity and mortality, but whether it is accompanied by a reproducible cardiac phenotype before overt cardiovascular disease (CVD) remains unclear. We aimed to characterize the cardiac phenotypic signature of MDD and its biological and clinical relevance.

Methods Using the UK Biobank, we integrated cardiovascular magnetic resonance (CMR), circulating biomarker and genomic data to assess MDD-associated cardiac remodelling across

82 standardized CMR traits (pre-imaging MDD n = 798; without MDD n = 35,659). We further examined symptom burden, illness duration, inflammatory–metabolic mediation, shared genetic architecture, and the prognostic value of selected right-heart traits in participants with MDD.

Results We identified a coherent, anatomically organised pattern of subclinical remodelling, with 43 of 82 CMR traits remaining significant after false discovery rate correction, characterized by smaller chamber volumes, reduced stroke and output indices, and increased myocardial wall thickness. Crucially, these alterations were not diffuse but exhibited a consistent right-heart predominance, with right ventricular and atrial volume and output traits showing the largest effect sizes across the CMR phenome; right ventricular stroke volume index showed one of the strongest associations (standardized $\beta = -0.230$, FDR-adjusted $P = 1.44 \times 10^{-9}$), and the reduction in right atrial minimum volume index was greater than that in its left-sided counterpart (βdiff = −0.094, 95% CI −0.175 to −0.014; Pdiff = 0.022). This phenotype scaled with depressive symptom severity, assessed using the Patient Health Questionnaire-2 (PHQ-2), and illness duration, and was partially mediated by immunometabolic dysregulation, including C-reactive protein, the triglyceride–glucose index and alkaline phosphatase. Genetic correlation, colocalization and Mendelian randomization analyses provided convergent evidence for shared genetic architecture between MDD and right-heart volume/output traits, with genetic signals observed for RVEDVi, RVESVi and RASVi but not their anatomically matched left-heart counterparts. Incorporating right-heart CMR traits into conventional risk models significantly enhanced long-term risk stratification for arrhythmic events.

Conclusions MDD is associated with a measurable cardiovascular endophenotype characterized by preferential right-heart involvement. These findings provide a cardiac manifestation of the brain–heart axis and a framework for investigating cardiovascular vulnerability in MDD.

Keywords: Major depressive disorder; cardiovascular magnetic resonance; cardiac remodelling; right heart; cardiovascular disease

Background

Major depressive disorder (MDD) is a leading contributor to global disease burden[1,2] and a major cause of disability and impaired quality of life, with consequences extending well beyond mental health[3,4]. Substantial evidence from prospective cohorts and meta-analyses has linked depression and greater depressive symptom burden to increased risks of coronary heart disease,

heart failure, stroke and cardiovascular death[5,6], as well as sudden cardiac death and selected arrhythmic outcomes[7]. Many of these associations persist after adjustment for lifestyle and conventional cardiovascular risk factors. Several systemic pathways, including inflammation, metabolic dysfunction, dysregulation of the hypothalamic–pituitary–adrenal axis and other neuroendocrine pathways, and autonomic imbalance, have been proposed to link depression with cardiovascular disease (CVD)[8-10]. However, these mechanisms do not establish how MDD is manifested in the heart itself. In individuals without overt CVD, whether MDD is associated with a reproducible pattern of subclinical cardiac structural and functional remodelling therefore remains unclear.

Previous cardiac imaging studies have reported depression-related differences in cardiac structure and function[11-13], but their findings have varied across study populations, definitions of depression, imaging modalities and phenotypic measures. Most prior research has focused on left ventricular structure and conventional measures of systolic or diastolic function, whereas the right ventricle and both atria have received relatively little systematic investigation[14]. Consequently, it remains uncertain whether MDD-associated cardiac alterations are diffuse or follow a chamber-selective pattern. Cardiovascular magnetic resonance (CMR) enables standardized and reproducible quantification of all four cardiac chambers, including chamber volumes, pumping function, myocardial geometry, strain and aortic characteristics[15,16], making it well suited to address this question. Although large-scale heart–brain imaging studies have linked mental health phenotypes to multiple cardiac traits[17], to our knowledge, no population-based study has systematically characterized clinically defined MDD across all four cardiac chambers in individuals without overt cardiovascular disease using a broad CMR phenome. Whether MDD is associated with a coherent and anatomically organised pattern of cardiac remodelling therefore remains to be established.

To address this gap, we sought to determine whether MDD is associated with a distinct and anatomically organised pattern of cardiac remodelling and to evaluate its potential biological and clinical relevance. We integrated clinical, CMR imaging and biomarker data from the UK Biobank with genome-wide association study (GWAS) summary statistics in a four-part analytical framework (Fig. 1). First, the MDD–CMR phenotypic association analysis characterized differences across 82 standardized CMR traits and evaluated their distribution across cardiac chambers and functional domains, consistency across symptom burden and illness duration, and robustness in sensitivity analyses. Second, the inflammatory–metabolic mediation analysis assessed whether circulating inflammatory and metabolic factors partly

explained the MDD–CMR associations. Third, the genetic analyses combined bidirectional Mendelian randomization, genome-wide genetic correlation and regional colocalization to examine shared genetic architecture and potential directionality. Fourth, the incremental prognostic value analysis assessed whether selected CMR traits added prognostic information for subsequent cardiovascular events beyond conventional risk factors in participants with MDD. Together, these analyses evaluated whether MDD is associated with anatomically selective rather than diffuse cardiac remodelling. Across these complementary analyses, we identified a cardiac remodelling pattern that was more prominent in right-heart than left-heart traits, particularly for chamber volume and stroke/output measures, highlighting preferential right-heart involvement in MDD.

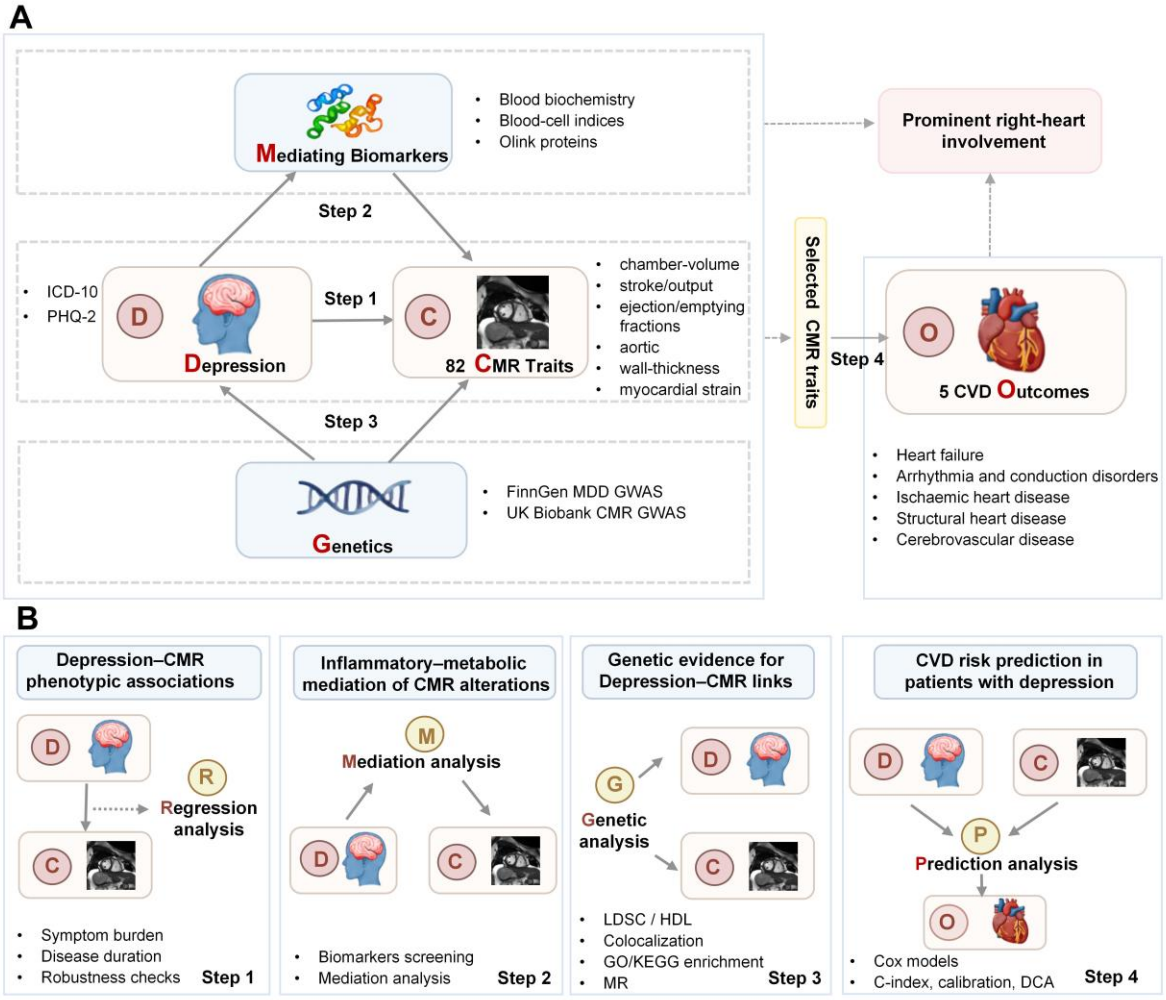


Fig. 1| Study overview and analytical workflow. Conceptual framework linking depression phenotypes, CMR traits, genetic evidence, mediation biomarkers and CVD outcomes (A). Analytical workflow comprising four steps: MDD-CMR phenotypic association analysis,

inflammatory-metabolic mediation analysis, genetic analyses of depression-CMR links, and CVD risk prediction in participants with MDD (B). CMR, cardiovascular magnetic resonance; CVD, cardiovascular disease; GWAS, genome-wide association study; PHQ-2, Patient Health Questionnaire-2.

Methods

Study design and participants

This study used data from the UK Biobank, a population-based prospective cohort of more than 500,000 participants recruited from 22 assessment centres across the United Kingdom between 2006 and 2010. The UK Biobank resource was used under application numbers 89757 and 681047; the UK Biobank study received ethical approval from the North West Multi-centre Research Ethics Committee (11/NW/0382), and all participants provided written informed consent[18].

Four analytical components were defined. MDD was ascertained from UK Biobank first-occurrence and diagnostic records using ICD-10 codes F32 and F33, with the first MDD date defined as the earliest recorded diagnosis across all available sources. (1) For the primary MDD–CMR association analysis, MDD status was determined before the CMR examination at imaging visit 2. After excluding participants with CVD before CMR, 36,457 of 39,675 participants remained, including 798 with pre-imaging MDD. (2) For mediation analyses, MDD occurring before the baseline assessment was used as the exposure to ensure that biomarker measurements preceded CMR. This cohort included 35,974 participants, of whom 315 had MDD. (3) Genetic analyses used FinnGen MDD GWAS summary statistics and GWAS data for 82 UK Biobank CMR traits, with additional published CMR GWAS datasets used in supporting analyses. (4) For prediction modelling, participants were required to have MDD before CMR and no CVD before or on the first MDD diagnosis date. The final cohort included 1,172 participants with MDD, among whom 121 developed incident CVD during follow-up. Fig. 2 summarizes the inclusion and exclusion criteria for the primary MDD – CMR association, mediation and prediction cohorts.

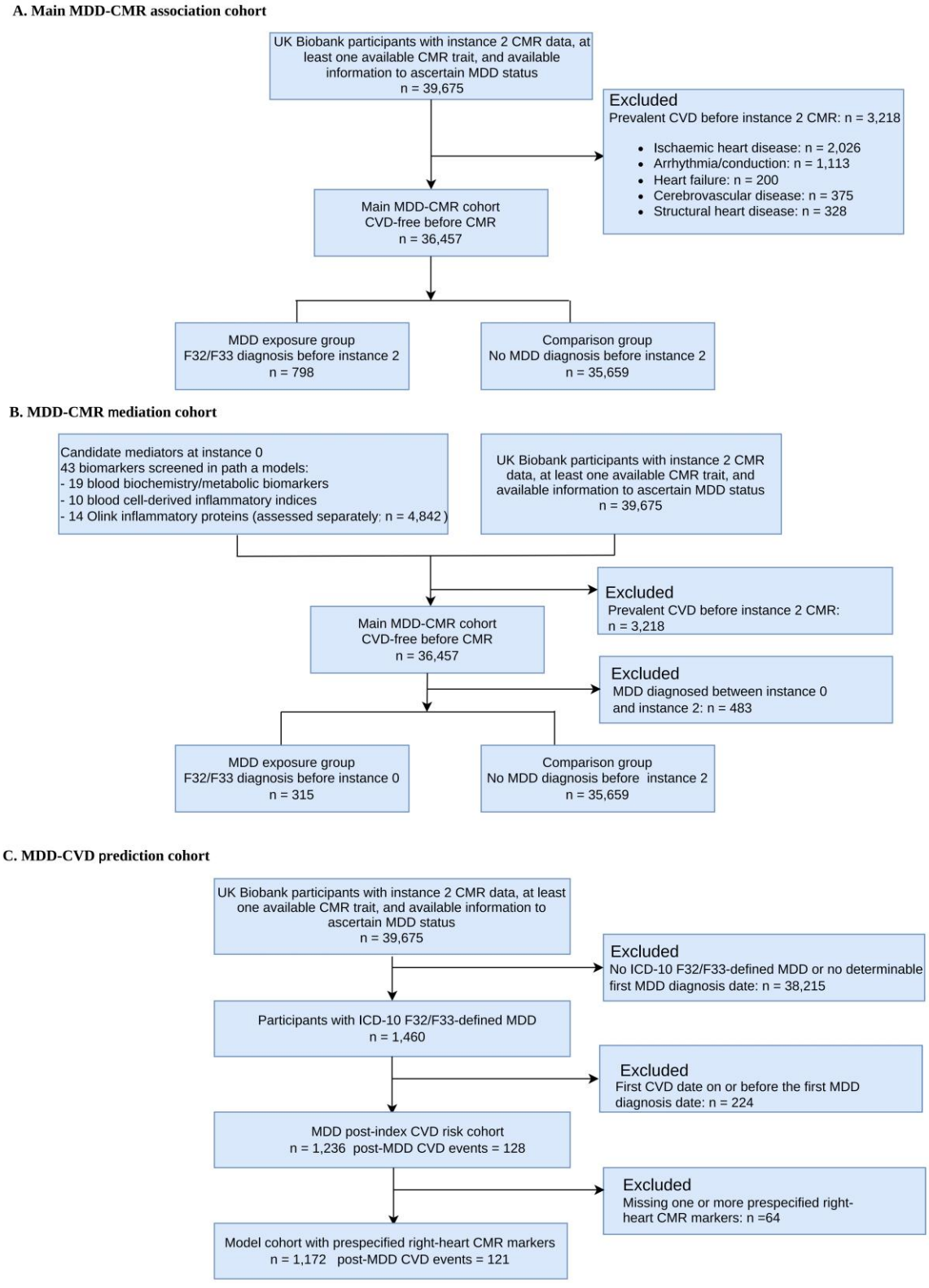


Fig. 2| Study cohort selection and analytical populations. Selection of the primary MDD–CMR association cohort after excluding participants with prevalent CVD before instance 2 CMR (A). Selection of the mediation cohort, requiring MDD exposure before baseline

biomarker assessment and subsequent CMR availability; Olink proteins were assessed separately because of the smaller sample size (B). Selection of the MDD–CVD prediction cohort, excluding participants with CVD on or before the first MDD diagnosis and those with missing prespecified right-heart CMR markers (C). CVD subtypes in (A) were not mutually exclusive. CMR, cardiovascular magnetic resonance; CVD, cardiovascular disease; MDD, major depressive disorder.

Regression analyses of MDD and CMR traits

A total of 82 CMR traits were included, derived from UK Biobank imaging data acquired and processed according to standardized imaging and quality-control procedures[19]. Traits were grouped into six domains: chamber volume, stroke/output volume, ejection/emptying fraction, aortic traits, wall thickness/hypertrophy and myocardial deformation. Volume-, mass- and area-based measures were indexed to body surface area where appropriate, and all CMR outcomes were z-score standardized before analysis. Detailed imaging protocols, trait definitions, indexing procedures and data-processing methods are provided in the Supplementary Methods and Table S1.

Multivariable linear regression was used to examine associations between pre-imaging MDD and each of the 82 standardized CMR traits. The primary model was adjusted for age at imaging, sex, ethnicity, educational attainment, Townsend deprivation index, body mass index, physical activity, smoking status, alcohol consumption and imaging centre. Standardized β coefficients and 95% confidence intervals were reported, with Benjamini–Hochberg FDR correction applied across the 82 CMR traits[16,20]. To assess potential right–left asymmetry, paired contrasts were additionally performed across six anatomically matched right–left trait pairs. Detailed covariate definitions and paired-comparison procedures are provided in the Supplementary Methods.

Robustness was evaluated using five independently extended covariate-adjusted models and one propensity-score overlap-weighted analysis[21]. The five models additionally considered cardiovascular risk factors, antidepressant use, mental health consultation, inflammatory–metabolic markers and metabolic syndrome, respectively; antidepressant use was further examined according to major medication classes. Right–left paired comparisons were repeated across all five extended covariate-adjusted models and the overlap-weighted analysis. Within participants with MDD, 1:1 propensity-score matching was performed for antidepressant use, mental health consultation and metabolic syndrome status, with antidepressant analyses additionally conducted by major medication class. Matched CMR traits were compared using

paired t-tests. Effect modification was evaluated by age, sex and metabolic syndrome status. Definitions of these clinical variables and further details of the sensitivity and propensity-score analyses are provided in the Supplementary Methods.

MDD duration was defined as the interval between the first recorded MDD diagnosis and the CMR examination and categorized as 0–2, 2–5, 5–10 and >10 years, with participants without MDD as the reference group. Restricted cubic spline models with four degrees of freedom were used to assess potential nonlinearity, with overall and nonlinear associations evaluated against covariate-only and linear-duration models, respectively. These analyses were interpreted as cross-sectional duration-stage differences rather than within-person longitudinal change.

PHQ-2 was used as a complementary measure of depressive symptom burden rather than as a diagnostic definition of MDD, as diagnostic records did not provide a consistent graded measure of depression severity[22]. PHQ-2 was analysed as both a continuous and categorical exposure, with score 0 as the reference category and scores 5–6 combined because of the smaller sample size. PHQ-2 derivation, coding and covariate definitions are provided in the Supplementary Methods.

Mediation analyses

To preserve temporal ordering, mediation analyses were restricted to MDD diagnosed before the baseline assessment (I0), with candidate biomarkers measured at baseline and CMR traits assessed subsequently at the imaging visit. We evaluated whether circulating inflammatory and metabolic biomarkers mediated the associations between MDD and CMR traits. Forty-three candidate mediators were screened, including 19 metabolic or biochemical markers, 10 inflammatory or hematological markers and 14 Olink inflammation-related proteins. Associations between pre-baseline MDD and each mediator were adjusted for baseline sociodemographic, lifestyle and clinical covariates, with FDR correction applied across all 43 markers[23-25].

Formal mediation analyses focused on ALP, CRP and TyG, which remained significantly associated with MDD after global FDR correction across the 43 candidate mediators. For each mediator–CMR pair, linear regression models were fitted for both the MDD–mediator and mediator–CMR pathways within a standard three-variable mediation framework. ACME, ADE, total effect and proportion mediated were estimated with 5,000 bootstrap resamples using the same covariate set. FDR correction was applied across 246 tests involving three mediators and

82 CMR traits. Mediation analyses were conducted in R version 4.5.3 using the mediation package (version 4.5.1)[26].

Mediation effects were also compared across six matched right–left CMR trait pairs using paired bootstrap contrasts with 5,000 resamples. Differences in absolute ACME between right- and left-heart traits were calculated for each mediator, with FDR correction applied across 18 comparisons. Olink proteins were analysed separately because of their smaller sample size. These analyses were considered exploratory and were FDR-corrected across all protein–CMR tests. Detailed biomarker preprocessing is provided in the Supplementary Methods.

Genetic analyses

Genetic analyses were performed using genome-wide association study (GWAS) summary statistics for MDD and cardiovascular magnetic resonance (CMR) traits. MDD summary statistics were obtained from the FinnGen Release 10 F5_DEPRESSIO phenotype, comprising 47,696 cases and 359,290 controls (total $N = 406{,}986$)[27]. The primary CMR dataset included 82 UK Biobank imaging-derived phenotypes from 31,875 participants of European ancestry, with variants restricted to minor allele frequency (MAF) >1%[28]. Additional published UK Biobank CMR GWAS datasets were used for supporting Mendelian randomization analyses of selected ventricular and myocardial-strain traits[29-31].

Genome-wide genetic correlations between MDD and the 82 CMR traits were estimated using linkage disequilibrium score regression (LDSC), implemented in the R package GenomicSEM (version 0.0.5; https://github.com/GenomicSEM/GenomicSEM)[32,33], and high-definition likelihood using the HDL R package (https://github.com/zhenin/HDL)[34]. LDSC analyses were restricted to HapMap3 variants and used European-ancestry LD scores, whereas HDL analyses used a UK Biobank imputed SVD LD reference matrix. Benjamini–Hochberg false discovery rate (FDR) correction was applied across the 82 CMR traits.

Bayesian colocalization analyses were performed using the R package coloc (version 5.2.3; https://chr1swallace.github.io/coloc/)[35,36] within ±500-kb windows around lead variants with $P < 1 \times 10^{-5}$ in either GWAS. Colocalization between MDD and CMR traits was assessed using the posterior probability of a shared causal variant (PP.H4), with PP.H4 ≥ 0.75 considered high-confidence evidence. To explore biological pathways underlying shared MDD–CMR loci, protein-coding genes within high-confidence colocalized regions were mapped using GENCODE v19 annotations[37]. Gene Ontology, KEGG and Reactome enrichment analyses were subsequently performed using g:Profiler through the gprofiler2 R package

(https://biit.cs.ut.ee/gprofiler/)[38-41], with Benjamini–Hochberg FDR-adjusted $P < 0.05$ considered statistically significant.

Bidirectional two-sample Mendelian randomization (MR) analyses were performed using the R package TwoSampleMR (version 0.7.0; https://mrcieu.github.io/TwoSampleMR/)[42] to evaluate potential directional relationships between MDD and CMR traits. Genetic instruments were selected at genome-wide significance ($P < 5 \times 10^{-8}$) and clumped at $r^2 < 0.001$ within a 10,000-kb window using the 1000 Genomes Phase 3 European reference panel[43]. The inverse-variance-weighted method was used as the primary estimator, complemented by weighted-median, MR-Egger, simple-mode, weighted-mode and maximum-likelihood methods[44,45]. Instrument strength was evaluated using F statistics. Heterogeneity and directional horizontal pleiotropy were assessed using Cochran's Q and the MR-Egger intercept, respectively, and leave-one-out analyses were performed within the same TwoSampleMR framework. MR-PRESSO (version 1.0; https://github.com/rondolab/MR-PRESSO)[46] was additionally used to assess horizontal pleiotropy and potential outlier effects. Benjamini–Hochberg FDR correction was applied across the 82 primary CMR outcomes, with nominal $P < 0.05$ considered suggestive evidence. Detailed quality-control criteria, genomic-coordinate harmonization, locus definitions, SNP harmonization, instrument selection and sensitivity analyses are provided in the Supplementary Methods.

Prediction modelling

Prediction modelling was performed using Cox proportional hazards analysis to assess whether right-heart CMR traits improved subsequent CVD risk prediction beyond clinical variables in participants with MDD. CVD outcomes were ascertained from UK Biobank records using a prespecified three-digit ICD-10 code dictionary. The primary outcome was the first incident CVD event after MDD diagnosis. Prespecified CVD subtypes included ischaemic heart disease (I20–I25), arrhythmias and conduction disorders (I44, I45 and I48), cerebrovascular disease (I60–I69), heart failure (I50), and structural heart disease (I05–I09 and I34–I37).

The prediction cohort comprised 1,172 participants with an available first MDD diagnosis date, CMR performed after MDD diagnosis, no CVD before or on the first MDD date, and complete RVEDVi, RVESVi and RASVi measurements. These three right-heart traits were selected based on consistent signals from the preceding phenotypic, mediation and genetic analyses. Follow-up began at the first MDD diagnosis and ended at the earliest of the first post-MDD CVD event, death, loss to follow-up or 30 September 2021.

We constructed two nested Cox prediction models to assess the incremental predictive value of right-heart CMR traits. The clinical model included age, sex, educational attainment, Townsend deprivation index, BMI, physical activity, smoking status, alcohol consumption, imaging centre, diabetes, systolic blood pressure and diastolic blood pressure. The extended CMR model additionally included standardized RVEDVi, RVESVi and RASVi.

Model performance was assessed using Harrell's C statistic. Performance gains were quantified by the ΔC statistic, with 95% confidence intervals and optimism-corrected estimates derived from 1,000 bootstrap resamples[47]. Royston's D and D-derived R^2 were also calculated[48]. At a fixed 5-year horizon, model performance was additionally evaluated using AUC, Brier score, integrated discrimination improvement (IDI), net reclassification improvement (NRI)[49] and decision-curve analysis (DCA)[50]. Model improvement was further evaluated using likelihood-ratio testing. For risk stratification, participants were divided into high- and low-risk groups according to the median risk score from the extended CMR model, and subsequent event risks were compared using Cox regression. Detailed definitions of the 5-year prediction metrics, NRI thresholds, decision-curve analysis and bootstrap procedures are provided in the Supplementary Methods.

Software and reproducibility

All statistical tests were two-sided unless otherwise specified. Continuous CMR traits were standardized before analysis, and associations were reported as standardized β coefficients with 95% confidence intervals. For analyses involving multiple parallel tests, *P* values were adjusted using the Benjamini–Hochberg false-discovery-rate procedure, with FDR-adjusted *P* values reported where appropriate. Mediation effects were estimated using 5,000 non-parametric bootstrap resamples, with FDR correction applied across the prespecified mediator–CMR tests. For prediction analyses, 95% confidence intervals and optimism-corrected performance estimates were obtained using 1,000 non-parametric bootstrap resamples; model improvement was additionally assessed using likelihood-ratio tests, discrimination and reclassification metrics, and decision-curve analysis at a fixed 5-year horizon.

Statistical analyses were performed primarily in R and Python. Mediation analyses were performed in R version 4.5.3 using the mediation package (version 4.5.1). Genetic analyses were performed using GenomicSEM (version 0.0.5), HDL, coloc (version 5.2.3), TwoSampleMR (version 0.7.0), MR-PRESSO (version 1.0), gprofiler2 and PLINK (version 1.90b7.2).

Results

Study sample characteristics

The study comprised three analysis-specific UK Biobank cohorts and a separate set of GWAS summary statistics. The MDD–CMR phenotypic association cohort included 36,457 participants without prevalent CVD at CMR, comprising 798 with MDD and 35,659 without a recorded MDD diagnosis. Compared with participants without MDD, those with MDD were younger (61.8 ± 7.6 versus 63.3 ± 7.5 years, P<0.001) and less often male (31.3% versus 46.4%, P<0.001). They also had a higher Townsend deprivation index (−1.3 ± 3.0 versus −1.9 ± 2.7, P<0.001), a higher body mass index (BMI) (27.9 ± 4.9 versus 26.3 ± 4.2 kg/m^2, P<0.001) and a greater prevalence of metabolic syndrome (24.4% versus 16.2%, P<0.001).

The inflammatory–metabolic mediation cohort included 35,974 participants, comprising 315 with MDD and 35,659 without MDD. Demographic differences were broadly similar to those observed in the phenotypic association cohort. Participants with MDD had higher levels of C-reactive protein (CRP; 1.8 ± 1.5 versus 1.4 ± 1.3 mg/L, $P < 0.001$), a higher triglyceride-glucose (TyG) index (8.7 ± 0.6 versus 8.6 ± 0.5, $P = 0.013$) and higher alkaline phosphatase (ALP; 83.4 ± 22.8 versus 79.1 ± 20.9, $P = 0.001$).

The genetic analyses used published GWAS summary statistics for MDD and CMR traits rather than a single participant-level cohort; baseline characteristics were therefore not applicable, and the contributing GWAS datasets and trait-specific sample sizes are detailed in the Methods.

The incremental prognostic value cohort comprised 1,172 participants with MDD, of whom 121 developed incident CVD over a median follow-up of 6.6 years. Compared with participants who remained free of CVD, those who developed CVD were older (64.6 ± 7.3 versus 61.6 ± 7.7 years, P<0.001), more often male (46.3% versus 31.3%, P=0.001), more likely to have diabetes (8.3% versus 3.1%, P=0.010) and had higher systolic blood pressure (136.4 ± 19.1 versus 131.5 ± 16.6 mmHg, P=0.007). Baseline characteristics of the three participant-level cohorts are provided in Table S2.

MDD-associated cardiac remodelling patterns

We examined associations between MDD and 82 CMR traits among 36,457 participants without prevalent CVD; definitions and classification of the CMR traits are provided in Table S1. After multivariable adjustment, 43 of 82 traits remained significant after false discovery rate correction (Fig. 3A, Fig. S1 and Table S3). Significant associations clustered in chamber-volume, stroke/output, wall-thickness and myocardial-strain domains. Specifically, 6 of 8

chamber-volume traits, all 5 stroke/output traits, 3 of 4 ejection or emptying fraction traits, 15 of 18 wall-thickness traits and 14 of 41 myocardial-strain traits were FDR-significant, whereas no aortic trait survived correction. Thus, MDD-associated CMR differences were concentrated in cardiac chamber size, stroke/output measures and myocardial geometry rather than aortic phenotypes.

At the individual-trait level, MDD was characterized by lower biventricular and biatrial volumes and reduced stroke/output measures, together with greater global and segmental wall thickness, whereas associations with ejection/emptying fraction and myocardial strain were more heterogeneous. Specifically, MDD was associated with lower right ventricular end-diastolic volume index (RVEDVi; standardized $\beta = -0.184$, FDR-adjusted $P = 8.12 \times 10^{-8}$) and left ventricular end-diastolic volume index (LVEDVi; $\beta = -0.169$, FDR-adjusted $P = 2.28 \times 10^{-6}$), while right ventricular end-systolic volume index (RVESVi) was also reduced ($\beta = -0.085$, FDR-adjusted $P = 0.014$) and left ventricular end-systolic volume index (LVESVi) showed a similar direction but did not survive FDR correction. Atrial volume traits showed a comparable pattern, with significant reductions in right atrial maximum volume index (RAmaxVi), right atrial minimum volume index (RAminVi) and left atrial maximum volume index (LAmaxVi). Stroke/output traits were consistently lower, with the largest estimates observed for right ventricular stroke volume index (RVSVi) ($\beta = -0.230$, FDR-adjusted $P = 1.44 \times 10^{-9}$) and left ventricular stroke volume index (LVSVi) ($\beta = -0.217$, FDR-adjusted $P = 1.53 \times 10^{-8}$), accompanied by lower right atrial stroke volume index (RASVi), left atrial stroke volume index (LASVi) and left ventricular cardiac index (LVCI). In contrast, wall-thickness traits were generally greater in MDD, including global wall thickness ($\beta = 0.140$, FDR-adjusted $P = 3.15 \times 10^{-6}$) and wall thickness at American Heart Association segment 7 (WT7; $\beta = 0.168$, FDR-adjusted $P = 9.02 \times 10^{-8}$), whereas left ventricular mass index (LVMi) was not FDR-significant. Myocardial-strain associations varied by strain component, with positive estimates for selected circumferential and longitudinal traits and negative estimates for radial strain traits. In paired-volume comparisons, right- and left-sided cardiac chambers showed concordant directions of association with MDD, with lower volume indices observed on both sides (Fig. 3B and Table S4). Right-heart volume traits generally exhibited numerically greater reductions than their left-heart counterparts across ventricular and atrial measures, including RVEDVi versus LVEDVi, RVESVi versus LVESVi, RAmaxVi versus LAmaxVi and RAminVi versus LAminVi. Among these paired comparisons, the difference in association magnitude between RAminVi versus left atrial minimum volume index (LAminVi) reached statistical significance ($\beta_{diff} = -0.094$, 95% CI −0.175 to −0.014, $P_{diff} = 0.022$). Together with the larger absolute effect

estimates observed for several right-heart traits in the primary analyses, these findings support a preferential involvement of right-heart volume remodelling in MDD-associated cardiac alterations.

Robustness of cardiac chamber and output associations

We performed five additional covariate-adjusted sensitivity analyses and one propensity score overlap-weighted analysis to evaluate the robustness of the observed MDD-associated CMR phenotype. Adjustment for cardiovascular risk factors retained all 43 primary FDR-significant traits, whereas adjustment for antidepressant use retained 19; importantly, key chamber-volume and stroke/output associations remained significant. Class-specific sensitivity analyses showed broadly similar patterns across antidepressant classes, with the greatest attenuation observed after adjustment for selective serotonin reuptake inhibitor (SSRI) use. Despite this attenuation, key chamber-volume and stroke/output associations remained FDR-significant. Adjustment for mental health consultation, inflammatory-metabolic markers and metabolic syndrome each retained 34 traits, and 39 of the 43 primary associations remained FDR-significant in the overlap-weighted analysis (Tables S5 and S6).

Paired right–left comparisons were also repeated in the cardiovascular-risk-factor-adjusted and overlap-weighted analyses. Consistent with the primary paired analysis, both models showed lower volume indices on the right and left sides of the heart, with numerically greater reductions in several right-heart traits. In particular, the RAminVi–LAminVi contrast remained nominally significant after adjustment for cardiovascular risk factors ($\beta_{diff} = -0.091$, 95% CI −0.171 to −0.011, $P_{diff} = 0.025$) and in the overlap-weighted analysis ($\beta_{diff} = -0.088$, 95% CI −0.158 to −0.017, $P_{diff} = 0.015$). These findings indicate that the greater reduction in right than left atrial minimum volume was consistently observed in the primary, cardiovascular-risk-factor-adjusted and overlap-weighted analyses (Table S7).

Stratified analyses by treatment and metabolic status

To examine whether treatment-related factors or metabolic status contributed to the observed cardiac phenotype, we performed internal comparisons among participants with MDD according to antidepressant use, mental health consultation and European-defined metabolic syndrome (Fig. 3C; Table S8). Within the MDD population, no CMR trait reached FDR significance in the matched comparisons by antidepressant use or mental health consultation, suggesting that these treatment-related factors were unlikely to account for the observed MDD-associated CMR pattern. Class-specific analyses similarly showed no FDR-significant CMR

differences for SSRI, SNRI, TCA or other N06AX antidepressant use (Fig. S2 and Table S6). In contrast, 20 of 82 CMR traits differed by metabolic syndrome status after FDR correction, indicating that cardiometabolic status may contribute to selected aspects of cardiac remodelling in MDD. Notably, right-heart traits including RVEDVi, RVESVi and RASVi did not differ according to metabolic syndrome status after FDR correction, suggesting that these right-heart alterations were not fully explained by coexisting metabolic abnormalities. Together, these findings suggest that treatment-related factors had limited influence on the observed CMR phenotype, whereas metabolic abnormalities may contribute to selected aspects of cardiac remodelling. Additional interaction analyses according to age, sex and metabolic syndrome status identified several nominally significant interactions (Table S9).

Disease-duration and symptom-burden analyses

We examined whether the identified CMR phenotype varied according to MDD duration and depressive symptom burden. Participants were classified according to the interval between first MDD diagnosis and CMR assessment as 0–2, 2–5, 5–10 and >10 years. CMR alterations were observed across multiple duration categories, but the distribution of affected traits differed by disease duration. In the shortest duration category (0–2 years), significant alterations were already observed in atrial traits, including reduced right atrial maximum volume index (RAmaxVi; β = −0.275, FDR-adjusted $P = 0.016$) and right atrial stroke volume index (RASVi; β = −0.297, FDR-adjusted $P = 0.011$), together with increased global wall thickness (β = 0.234, FDR-adjusted $P = 0.008$), whereas the corresponding left-heart estimates were generally smaller. With increasing MDD duration, abnormalities progressively extended to the left heart. For example, RVEDVi showed an FDR-significant association in the 2–5-year category (β = −0.217, $P = 0.001$, FDR-adjusted $P = 0.021$), whereas LVEDVi showed an FDR-significant association later in the 5–10-year category (β = −0.189, $P = 0.002$, FDR-adjusted $P = 0.026$). In the >10-year category, several left-heart volume and output traits showed effect estimates comparable to or greater than their right-heart counterparts. Duration-stage-specific right–left paired comparisons further showed a nominally greater reduction in RAminVi than LAminVi in the 0–2-year category (β_{diff} = −0.200, 95% CI −0.387 to −0.013, $P_{diff} = 0.036$). Together, these duration-specific patterns suggest that right-heart alterations may emerge earlier in MDD, followed by progressively greater left-heart involvement with longer disease duration (Fig. S3 and Table S10). Restricted cubic spline analyses showed nominal evidence of nonlinearity for right atrial emptying fraction (RAEF) and RASVi (nonlinearity $P = 0.027$ and 0.011, respectively).

To complement diagnosis-based analyses, we evaluated depressive symptom burden using baseline PHQ-2 scores. Higher PHQ-2 scores were associated with lower chamber-volume indices, with more negative associations generally observed for right-sided than left-sided traits. In continuous models, mean standardized β values were −0.038 for right-sided chamber indices and −0.030 for left-sided chamber indices (both $P < 0.001$). Stroke/output indices showed a similar pattern, with higher PHQ-2 scores more strongly associated with lower right-sided stroke/output indices (mean standardized $\beta = -0.042$) than with left-sided traits (mean standardized $\beta = -0.038$; both $P < 0.001$). Global and segmental wall-thickness traits also showed positive associations with PHQ-2 score (Fig. 3D). Category-specific analyses showed a broadly graded pattern of smaller chamber volumes and lower stroke/output indices with increasing PHQ-2 score, whereas wall-thickness measures showed positive associations that were most pronounced around a PHQ-2 score of 3 (Fig. 3E). Paired trait analyses further showed that right-heart estimates were generally more negative than their left-heart counterparts across several PHQ-2 categories, particularly for atrial volume traits (Fig. S4). Together, these findings demonstrate a symptom-burden-related CMR pattern consistent with that observed for ICD-10-defined MDD, characterized by smaller chamber volumes, reduced stroke/output indices and increased myocardial wall thickness (Table S11).

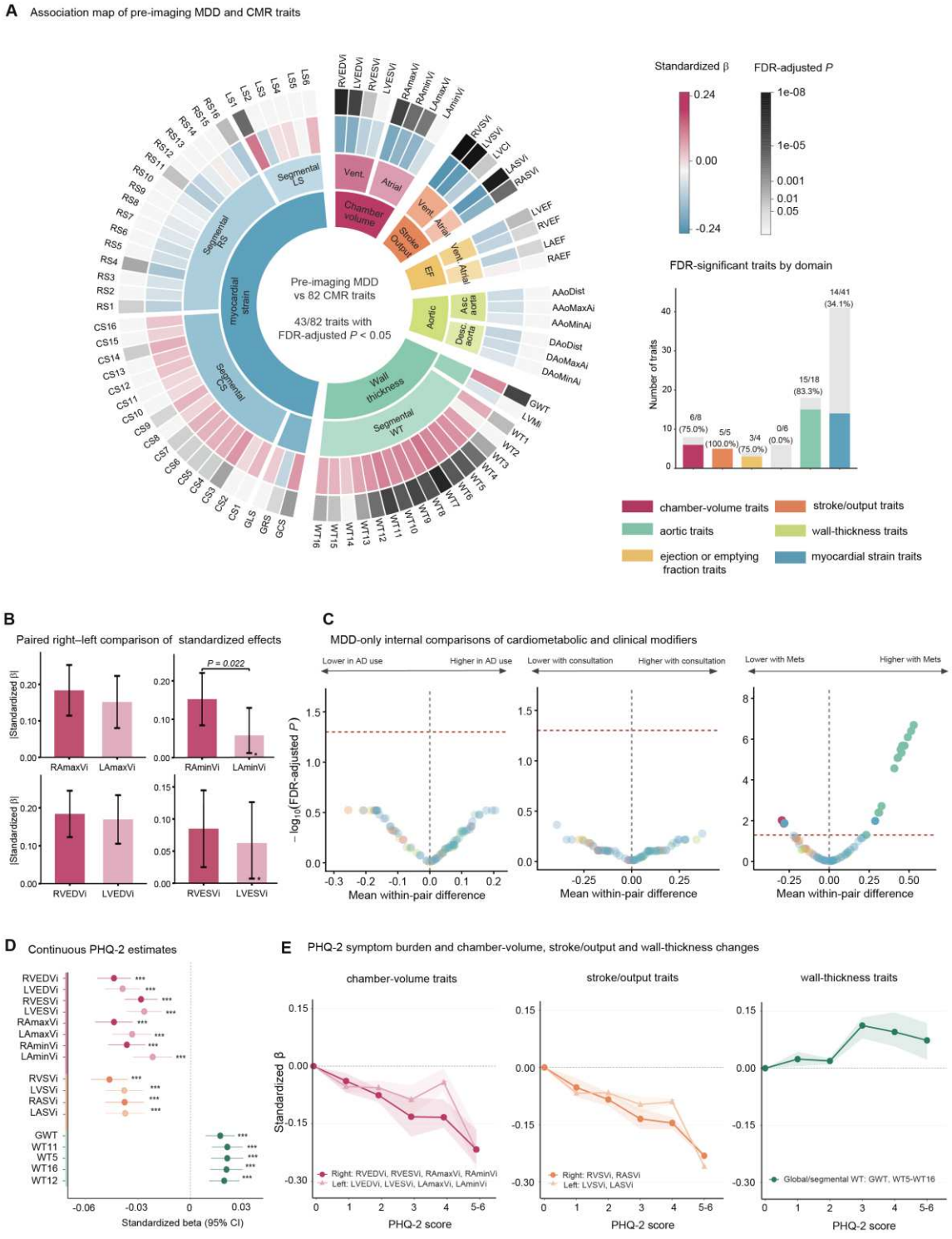


Fig. 3| Associations of pre-imaging MDD, clinical modifiers and depressive symptom burden with CMR traits. (A) Circular map of associations between pre-imaging MDD and 82 CMR traits. Outer tiles show standardized β estimates and the outer ring shows FDR-adjusted *P* values; bars summarize the number of FDR-significant traits by domain. (B) Paired right–left comparisons of absolute standardized β estimates for four matched chamber-volume pairs, with 95% CIs; *P* values indicate paired differences in effect magnitude. (C) Effect–significance plots

from 1:1 propensity-score-matched comparisons by antidepressant use, mental health consultation and metabolic syndrome status. Colors denote CMR domains; stronger colors indicate FDR-adjusted $P < 0.05$. (D) Continuous associations of PHQ-2 score with selected CMR traits; points and lines show standardized β estimates and 95% CIs. *, ** and *** indicate FDR-adjusted $P < 0.05$, <0.01 and <0.001, respectively. (E) Associations across PHQ-2 categories (0, 1, 2, 3, 4 and 5–6); lines show mean standardized β estimates and shaded areas the range across component traits. β, beta coefficient; CI, confidence interval; FDR, false discovery rate; MetS, metabolic syndrome; PHQ-2, Patient Health Questionnaire-2.

Biomarker mediation of cardiac volume and output alterations

We screened 43 prespecified circulating biomarkers as potential mediators of MDD-associated CMR alterations. After FDR correction, MDD was associated with higher levels of alkaline phosphatase (ALP; standardized β = 0.207, 95% CI 0.096–0.317, FDR-adjusted P = 0.010), C-reactive protein (CRP; β = 0.170, 95% CI 0.062–0.277, FDR-adjusted P = 0.028) and triglyceride–glucose (TyG) index (β = 0.169, 95% CI 0.063–0.276, FDR-adjusted P = 0.028). These three biomarkers were carried forward to the primary mediation analyses (Fig. 4A; Table S12).

Across 246 primary mediation tests, TyG showed the broadest pattern, with FDR-significant average causal mediation effects (ACMEs) for 66 of 82 CMR traits, compared with 46 traits for ALP and 40 traits for CRP (Fig. 4B). Mediation was most consistent for cardiac volume and output phenotypes: all 24 chamber-volume mediator–trait combinations and 14 of 15 stroke/output combinations had FDR-adjusted P < 0.05. The ACMEs were uniformly negative, consistent with these biomarkers partly mediating the lower chamber-volume and stroke/output measures associated with MDD. TyG also showed widespread mediation of wall-thickness alterations, with significant effects for 17 of 18 traits. Across chamber-volume and stroke/output phenotypes, the absolute average direct effects (ADEs) were generally larger than the corresponding ACMEs, indicating that a substantial component of the MDD–CMR associations remained beyond the measured inflammatory and metabolic mediators (Table S13). The domain-level distribution of FDR-significant mediation effects across ALP, CRP and TyG is summarized in Fig. S5.

Paired right–left analyses showed consistently larger absolute ACMEs for RAmaxVi, RAminVi and RASVi than for their corresponding left-atrial traits across ALP, CRP and TyG, with all nine comparisons remaining significant after FDR correction (Fig. 4C; Table S13). These

findings indicate stronger inflammatory–metabolic mediation of right-atrial volume and output alterations than of their corresponding left-atrial measures. However, the absolute indirect effects were modest. This pattern is compatible with the absence of significant metabolic-syndrome-related differences in RVEDVi, RVESVi and RASVi within participants with MDD (Fig. 3C), and provides complementary evidence for greater inflammatory–metabolic involvement in right- than left-heart remodelling.

Because Olink inflammatory proteins were available in a smaller subset, they were analyzed separately across the 82 CMR traits. Interleukin-6 (IL-6) was the only Olink measure with mediation effects that survived global FDR correction, spanning chamber-volume, stroke/output, wall-thickness/LV-mass and aortic domains. These findings were considered exploratory.

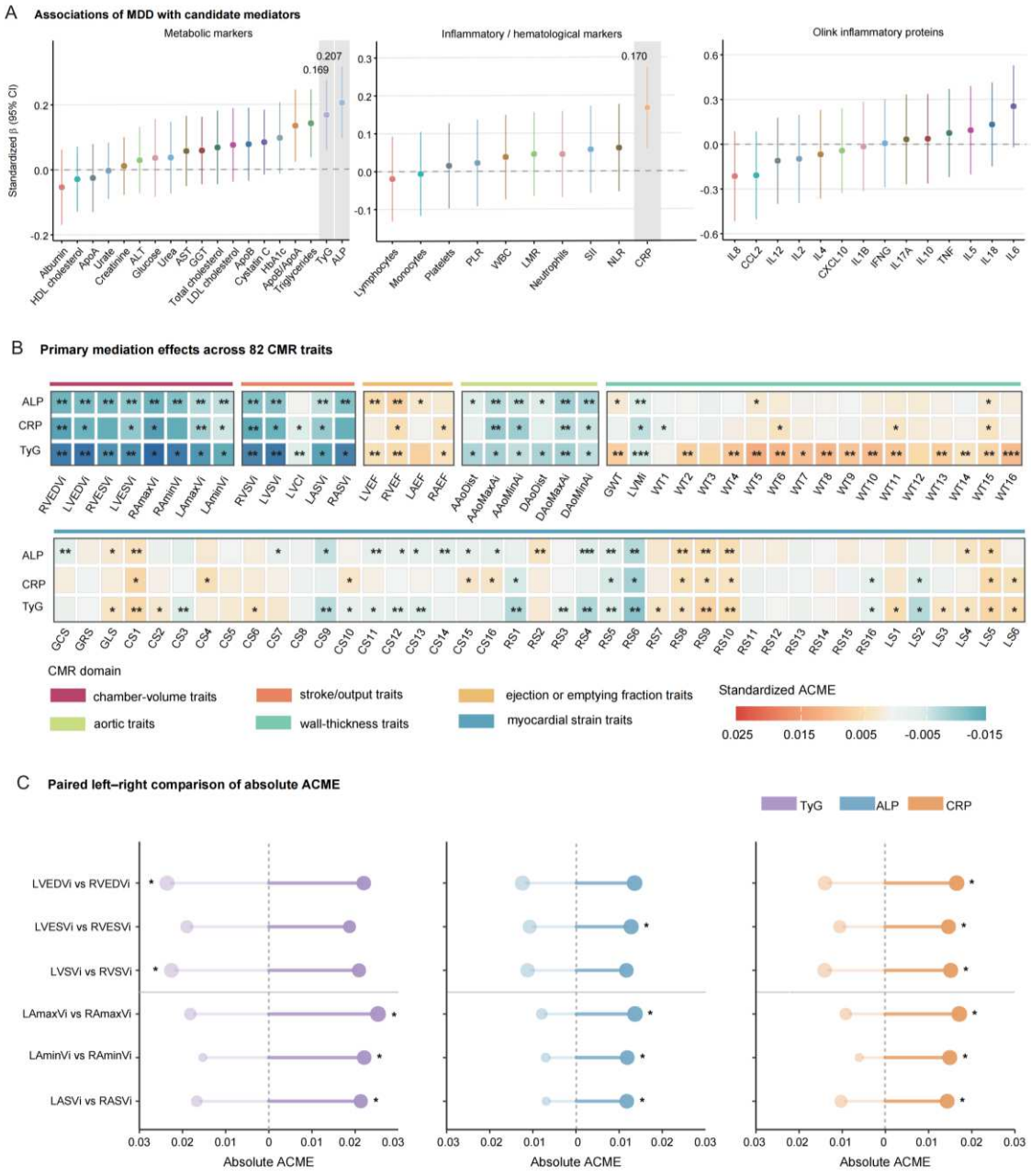


Fig. 4| Biomarker mediation evidence linking MDD to CMR alterations. Associations of MDD with 43 candidate circulating mediators, grouped as metabolic markers, inflammatory or hematological markers, and Olink inflammation-related proteins (A). Points and vertical lines show standardized β estimates for path a and 95% confidence intervals (CIs), respectively. Shaded areas indicate biomarkers carried forward to the primary mediation analyses. Standardized average causal mediation effect (ACME) estimates for ALP, CRP and TyG across 82 cardiovascular magnetic resonance (CMR) traits, ordered by CMR domain (B). Tile color represents signed standardized ACME. *FDR-adjusted $P < 0.05$; **FDR-adjusted $P < 0.01$; ***FDR-adjusted $P < 0.001$ across the 246 primary mediation tests. Mirrored paired lollipop

plots comparing absolute ACME (|ACME|) between six matched left- and right-heart CMR trait pairs for TyG, ALP and CRP (C). Left-heart traits are plotted on the left and the corresponding right-heart traits on the right. *FDR-adjusted $P < 0.05$ for paired left-right differences in |ACME|; symbols are placed beside the trait with the larger |ACME|. ACME, average causal mediation effect; ALP, alkaline phosphatase; CRP, C-reactive protein; TyG, triglyceride-glucose index.

Shared genetic liability and potential effector genes

To investigate whether the observed MDD-associated CMR phenotype reflected shared genetic architecture and potential directional relationships, we integrated genome-wide genetic correlation, trait-trait colocalization, functional annotation and Mendelian randomization analyses (Fig. 5). Genetic analyses primarily used GWAS summary statistics for MDD and 82 CMR traits from established large-scale datasets, with independent external GWAS resources used for supplementary validation of selected findings (Table S14).

Genome-wide genetic correlation analyses using linkage disequilibrium score regression (LDSC) and high-definition likelihood (HDL) identified negative genetic correlations between MDD and several right-heart volume/output traits (Fig. 5A). Using UK Biobank-derived CMR GWAS summary statistics, genetic correlation signals were observed for RVEDVi, RVESVi and RASVi, while the anatomically matched left-heart traits showed no corresponding associations. Additional nominal genetic correlation signals were also observed for several myocardial-strain traits (Fig. S6 and Table S15). These findings suggested shared polygenic architecture between MDD and the identified cardiac remodelling phenotype, with a preferential right-heart pattern.

Trait-trait colocalization across 82 CMR traits identified five high-confidence regions (PP.H4 ≥ 0.75) shared between MDD and CMR phenotypes (Fig. 5B). These included RASVi (PP.H4 = 0.919), RAminVi (PP.H4 = 0.832), regional circumferential strain at AHA segment 4 (CS4), and regional wall thickness at AHA segments 2 and 9. Regional association plots further illustrated the shared genetic loci underlying the two right-heart traits, RASVi and RAminVi (Fig. 5C), with regional plots for all five high-confidence loci presented in Fig. S7. Detailed locus coordinates, lead variants, analysed single-nucleotide polymorphisms, posterior probabilities, complete colocalization results and functional annotations are provided in Table S16.

Functional annotation of 54 protein-coding genes mapped from these high-confidence colocalized loci revealed seven FDR-significant Gene Ontology terms related to microtubule polymerization/depolymerization, protein localization to microtubules and protein crosslinking/organization (Fig. 5D).

Finally, bidirectional two-sample Mendelian randomization was performed to evaluate potential directional relationships between MDD and CMR traits (Fig. 5E). Forward MR using 17 independent genome-wide significant MDD instruments (mean F-statistic = 37.03) revealed nominal associations with lower RVEDVi ($\beta = -0.072$, nominal P = 0.022), RVESVi ($\beta = -0.066$, nominal P = 0.046) and RASVi ($\beta = -0.131$, nominal P = 0.022). A nominal association was also observed for regional radial strain at AHA segment 16 ($\beta = -0.121$, nominal P = 0.007). Full MR results and SNP-level supporting analyses are provided in Fig. S8 and S9.

Sensitivity analyses provided no evidence of substantial directional horizontal pleiotropy, with non-significant MR-Egger intercept tests across the four nominally associated traits (P = 0.159–0.608). Cochran's Q tests did not indicate strong heterogeneity overall, although RASVi was close to the nominal threshold (Q = 26.26, P = 0.0505). MR-PRESSO global tests detected no significant outlier effects (P = 0.059–0.751). Leave-one-out analyses further showed that the estimates were not materially driven by any single MDD genetic instrument (Fig. S10). Two additional nominal forward MR associations with ascending aortic maximum area index (AAoMaxAi) and ascending aortic minimum area index (AAoMinAi) were not prioritized because they showed limited consistency across complementary MR methods and leave-one-out analyses.

Reverse Mendelian randomization (MR) analyses provided no evidence that the evaluated CMR traits increased MDD risk (Fig. S11). Supporting analyses using three additional published CMR GWAS datasets yielded directionally consistent results for RVEDVi, RVESVi and RVSVi. Corresponding forward and reverse MR estimates, SNP-level associations and leave-one-out analyses are presented in Figs. S12–S15.

Across complementary genetic analyses, convergent signals were concentrated in right-heart volume and output traits. Genetic correlation, colocalization and Mendelian randomization analyses highlighted right atrial and right ventricular phenotypes, whereas corresponding evidence for matched left-heart volume traits was limited. Overall, the genetic findings were consistent with the preferential right-heart pattern observed in the phenotypic analyses. Complete bidirectional MR results, including the full primary forward MR scan, sensitivity

diagnostics, reverse MR analyses and supporting analyses using external CMR GWAS datasets, are provided in Table S17.

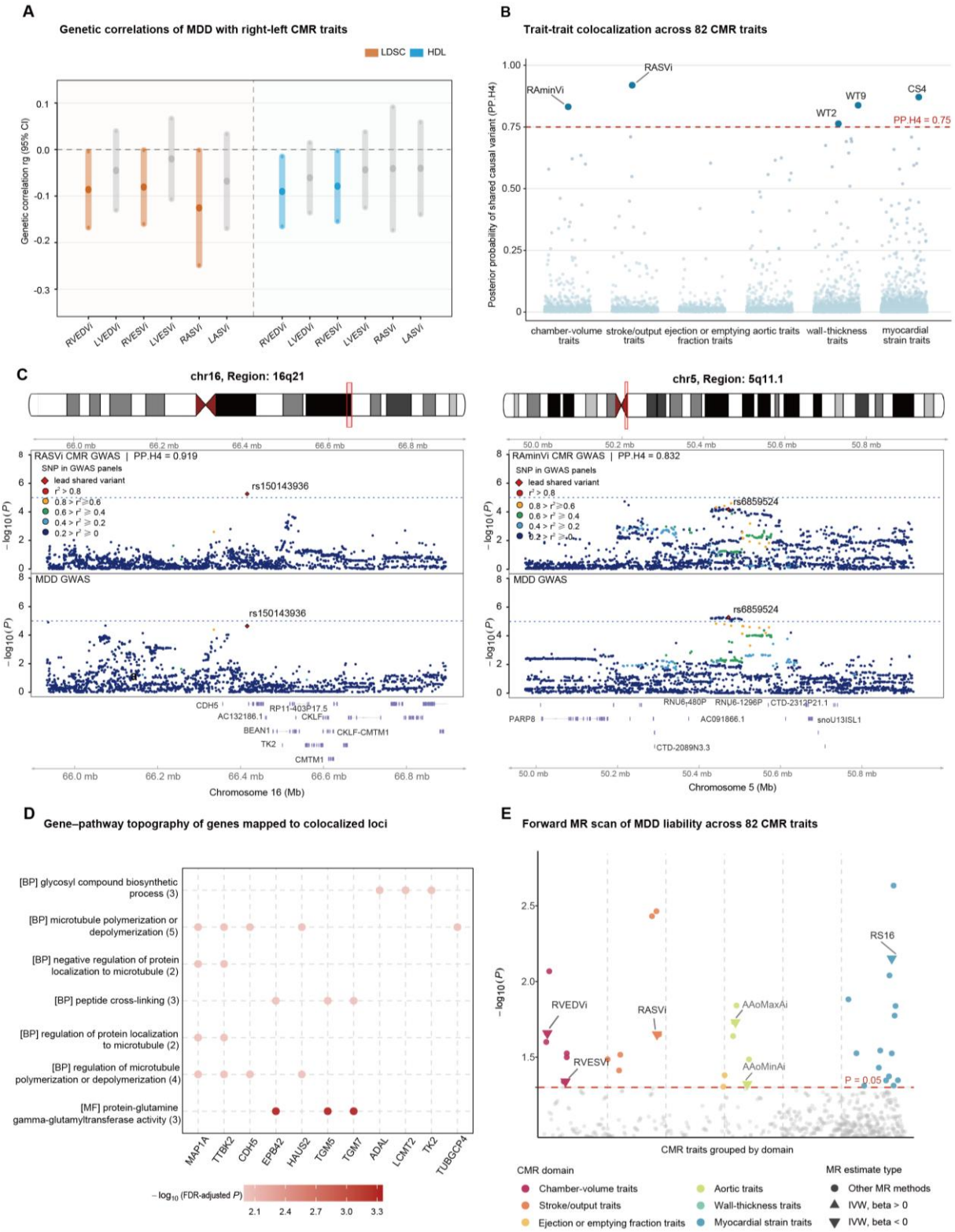


Fig. 5| Shared genetic architecture and directional genetic evidence linking MDD with CMR traits. (A) Genetic correlations between MDD and selected nominally significant CMR

traits estimated by LDSC and HDL; points and error bars show *r*g estimates and 95% CIs. (B) Trait–trait colocalization scan across 82 CMR traits; high-confidence signals are labelled. (C) Regional association plots for RASVi and RAminVi, showing CMR and MDD association signals, gene models and the $P = 1 \times 10^{-5}$ threshold. (D) Gene–GO term topography for protein-coding genes mapped to high-confidence colocalized loci; numbers indicate contributing genes. (E) Forward MR scan of genetically predicted MDD liability across 82 CMR traits. The dashed line marks nominal $P = 0.05$; triangles denote IVW estimates, with direction indicating effect sign, and circles denote other MR methods. GO, Gene Ontology; GWAS, genome-wide association study; HDL, high-definition likelihood; IVW, inverse-variance weighted; LDSC, linkage disequilibrium score regression; MR, Mendelian randomization; PP.H4, posterior probability for a shared causal variant.

Incremental prognostic value of right-heart CMR traits for arrhythmia in MDD

Based on the convergent phenotypic, mediation and genetic evidence, we selected RVEDVi, RVESVi and RASVi to examine whether the identified right-heart phenotype carried prognostic information beyond conventional cardiovascular risk factors among 1,172 participants with MDD. During a median follow-up of 6.6 years, 121 incident composite cardiovascular disease events occurred. Incorporating the three right-heart CMR traits alongside conventional clinical risk factors resulted in only a modest increase in overall discrimination for composite cardiovascular disease, with the bootstrap-corrected concordance index (C-index) increasing from 0.634 (95% CI 0.589–0.680) to 0.639 (95% CI 0.593–0.686) (Table S18). Five-year decision-curve analysis further evaluated the clinical net benefit of the extended model (Fig. S16).

The additional prognostic information carried by the right-heart traits was most evident for arrhythmic outcomes. Among 43 incident arrhythmic events, incorporation of RVEDVi, RVESVi and RASVi increased the bootstrap-corrected C-index from 0.663 (95% CI 0.571–0.734) to 0.701 (95% CI 0.613–0.769), corresponding to a ΔC-index of 0.038 (95% CI −0.011 to 0.070), and significantly improved model fit (likelihood-ratio test P = 0.016). Consistent with this finding, risk stratification incorporating the right-heart traits identified a subgroup with substantially higher subsequent arrhythmic risk (HR = 2.87, 95% CI 1.80–4.58). Among the three traits, RVESVi contributed most strongly to the observed incremental prognostic information. CVD subtype-specific prediction performance, C-index comparisons and risk-stratification results are presented in Table S19 and Figs. S17-S18.

Together, these analyses indicate that the right-heart volume and output traits identified throughout the preceding phenotypic, mediation and genetic analyses are not merely cross-sectional imaging correlates of MDD, but also carry additional information about subsequent cardiovascular risk beyond conventional clinical factors. The concentration of this incremental information in arrhythmic outcomes further supports right-heart remodelling as a clinically relevant and distinctive component of the MDD-associated cardiac phenotype.

Discussion

In this large-scale, population-based CMR study of 36,457 individuals without overt CVD, MDD was associated with smaller chamber volumes, reduced stroke and output indices, and greater myocardial wall thickness across 82 standardized CMR traits, with preferential involvement of right-heart volume and output traits. This phenotype varied with depressive symptom burden and illness duration, was partly mediated by inflammatory and metabolic dysregulation, and was supported by convergent genetic evidence. Given the reported cardiovascular effects of SSRIs[10,51], the greater attenuation after SSRI adjustment was notable, although key chamber-volume and stroke/output associations persisted. Collectively, these observations identify a cardiovascular endophenotype of MDD, providing a measurable anchor for the brain–heart axis and extending current models of depression as a systemic illness.

The consistent preferential involvement of right-heart chambers is the most distinctive feature of this endophenotype. Although formal chamber-specific interaction tests did not survive stringent multiple-comparison correction, the right-heart predominance recurred across primary analyses, sensitivity models, symptom-burden gradients, illness-duration strata, and genetic scans—arguing strongly against a chance finding. This regional vulnerability is biologically plausible. In contrast to the thick-walled left ventricle, which is optimized for high-pressure systemic circulation, the right ventricle and atrium are low-pressure, high-compliance structures[52,53]. This intrinsic architecture renders them exquisitely sensitive to subclinical elevations in pulmonary vascular impedance and fluctuations in cardiac preload[54,55]. In the context of MDD, chronic sympathovagal imbalance and pro-inflammatory states may induce subtle but persistent increases in right-heart afterload or reductions in effective venous return[8,56,57]. Our findings suggest that these systemic stressors manifest preferentially in the right heart, where the relative lack of muscular reserve makes structural and functional remodelling detectable earlier than in the more robust left-sided chambers.

Our mediation and genetic results add mechanistic depth to this cardiovascular endophenotype. Inflammatory and metabolic markers—particularly C-reactive protein, the triglyceride-glucose

index and alkaline phosphatase—consistently mediated a portion of the depression–cardiac association, suggesting that immunometabolic dysregulation contributes to, but does not fully account for, the observed cardiac phenotype[23,24]. Independent genetic analyses further revealed shared polygenic architecture between depression and right-heart volume/output traits, with high-confidence colocalization at several loci and functional annotation pointing toward microtubule-related[58,59] and structural remodelling processes[60]. Although individual Mendelian randomization estimates did not survive stringent correction across all 82 traits and should be interpreted as suggestive rather than definitive, the directional consistency across multiple complementary genetic modalities—forward and reverse MR, LDSC, HDL and colocalization—strengthens the hypothesis that depression and cardiac remodelling share, at least in part, common molecular origins. These convergent lines of evidence provide a candidate biological framework for future experimental investigation.

From a clinical perspective, the modest incremental prognostic value of right-heart CMR traits for composite cardiovascular disease (ΔC-index = 0.005) indicates that this endophenotype is not a broad-spectrum screening tool. However, exploratory subtype analyses revealed a more pronounced prognostic signal specifically for arrhythmic events (ΔC-index = 0.038; LRT P = 0.016), consistent with the pathophysiological link between depressive autonomic dysregulation, subclinical structural remodelling and pro-arrhythmic substrates. MDD has been associated with sympathetic activation, reduced parasympathetic modulation and impaired heart-rate variability, all of which may increase triggered activity, conduction heterogeneity and repolarization instability[56,61]. These autonomic abnormalities may interact with the subclinical right-heart structural changes identified in the present study, thereby creating a cardiac substrate particularly susceptible to arrhythmogenesis and potentially defining an arrhythmia-prone biotype within MDD, rather than serving simply as a general cardiovascular risk marker. Notably, RVESVi contributed most to the incremental prognostic signal; by reflecting residual ventricular volume after systolic contraction, RVESVi may capture impaired right-ventricular emptying, mechanical loading and electromechanical instability more sensitively than end-diastolic volume alone. Importantly, our results suggest that cardiac imaging could eventually serve as a quantitative tool for the biological staging of MDD. By integrating cardiac phenotypes with traditional psychiatric assessments, clinicians may better characterize the systemic progression of the disorder, identifying a “cardiovascular-vulnerable” biotype of depression. Future computational frameworks integrating cardiac imaging, psychiatric phenotypes, biomarkers and genomic information may further refine the characterization of cardiovascular vulnerability in MDD[62-66]. This biological staging

framework could refine how we monitor long-term physical health trajectories in psychiatric populations and provide a basis for integrating cardiovascular-protective interventions into precision mental health strategies.

Several limitations should be acknowledged. First, despite multiple complementary genetic analyses, the observational design and suggestive nature of the MR findings preclude definitive causal inference; we cannot exclude the possibility that unmeasured confounders or reverse causation contribute to the observed associations. Second, UK Biobank participants are predominantly of European ancestry and healthier than the general population, which may limit generalizability to more severe, treatment-resistant, or ethnically diverse psychiatric populations[67]. Third, depression was ascertained via healthcare records and a brief symptom questionnaire (PHQ-2), lacking repeated, fine-grained assessments of severity, treatment response, and within-person trajectories; our findings may not extend to subclinical depressive states or to MDD with psychotic features. Fourth, concurrent neuroimaging, autonomic, or neuroendocrine measurements were unavailable, preventing direct characterization of the brain-to-heart pathways that likely drive the observed remodelling; the autonomic and pulmonary mechanisms underlying right-heart predominance remain hypothetical. Fifth, the incremental prognostic value for overall CVD was modest, underscoring that this endophenotype currently informs biological understanding more than immediate wide-scale clinical risk stratification. Finally, CMR was performed at a single time point, precluding assessment of within-person cardiac remodelling trajectories and their temporal relationship to depressive episodes.

Conclusions

In conclusion, this study provides evidence that MDD is accompanied by a structured, right-heart-predominant pattern of subclinical cardiac remodelling, supported by inflammatory, metabolic and convergent genetic data. This cardiovascular endophenotype offers a cardiac manifestation of the brain–heart axis and may serve as a foundation for future precision mental health research, in which cardiac imaging phenotypes help stratify cardiovascular vulnerability—particularly arrhythmic risk—and guide mechanistic studies linking psychiatric illness to physical disease. The framework presented here provides a starting point for interdisciplinary efforts bridging psychiatry, cardiology, immunology and neuroscience.

List of abbreviations

ACME, average causal mediation effect; ADE, average direct effect; ALP, alkaline phosphatase; BMI, body mass index; CMR, cardiovascular magnetic resonance; CRP, C-reactive protein; CVD, cardiovascular disease; DCA, decision-curve analysis; FDR, false discovery rate; GWAS, genome-wide association study; HDL, high-definition likelihood; ICD-10, International Classification of Diseases, Tenth Revision; IDI, integrated discrimination improvement; IVW, inverse-variance weighted; LD, linkage disequilibrium; LDSC, linkage disequilibrium score regression; MAF, minor allele frequency; MDD, major depressive disorder; MR, Mendelian randomization; NRI, net reclassification improvement; PHQ-2, Patient Health Questionnaire-2; PP.H4, posterior probability for a shared causal variant; SNP, single-nucleotide polymorphism; TyG, triglyceride-glucose index.

Declarations

Ethics approval and consent to participate The UK Biobank study received ethical approval from the North West Multi-centre Research Ethics Committee (11/NW/0382), and all participants provided written informed consent. The UK Biobank resource was used under application numbers 89757 and 681047.

Consent for publication Not applicable.

Availability of data and materials The individual-level data analyzed in this study were obtained from the UK Biobank under application numbers 89757 and 681047 and are available to approved researchers through the UK Biobank standard access procedure (https://www.ukbiobank.ac.uk/use-our-data/apply-for-access/). All GWAS summary statistics used in this study are publicly available. MDD GWAS summary statistics were obtained from FinnGen Release 10 (F5_DEPRESSIO; https://finngen.gitbook.io/documentation/r10/data-download). Summary statistics for the primary 82 UK Biobank CMR traits were obtained from the Zenodo repository (https://zenodo.org/records/7239166), and additional published CMR GWAS datasets were obtained from the Cardiovascular Disease Knowledge Portal (https://cvd.hugeamp.org/downloads.html), the NHGRI-EBI GWAS Catalog (https://www.ebi.ac.uk/gwas/docs/file-downloads), and the Oxford HCM resource (https://www.chg.ox.ac.uk/research/research-groups/watkins-group-inherited-heart-muscle-disease-group-1/hcm/tadros/). Detailed data sources, phenotype definitions, sample sizes and accession numbers are provided in Table S14. The analysis code is publicly available at https://github.com/nancy70-zdn/MDD_CMR.

Competing interests The authors declare that they have no competing interests.

Funding This work was supported by the National Key Research and Development Program of China (Grant No. 2024YFC3506100), the Technical Innovation Key Project of Zhejiang Province (2025C01103), the National Natural Science Foundation of China (Grant Nos. 82272129 and 82572380), and the Natural Science Foundation of Zhejiang Province (LHZSZ25H090002). The funders had no role in study design, data collection and analysis, decision to publish, or preparation of the manuscript.

Authors' contributions D.Z. performed data analyses, prepared figures and tables in the main text and most of those in the Supplementary Information, and wrote the majority of the manuscript. Z.D. contributed to the design of the analytical strategy, drafted sections of the manuscript, and participated in critical revision of the manuscript. K.W. contributed to the preparation of figures and tables in the Supplementary Information. Y.H. and K.Z. contributed to data analysis and discussions regarding the overall structure of the manuscript. Y.W. provided guidance on medical and clinical aspects of the study. Y.M. and Z.L. provided guidance on data analysis methods. M.P., J.S., Z.T., M.Y. and F.Y. contributed to discussions regarding the overall logic and structure of the study and manuscript. J.Z. provided clinical guidance from the perspective of psychiatry and mental health. H.Z. provided clinical guidance from the perspective of cardiovascular medicine. F.W. provided guidance on the overall study concept and research strategy. H.M. and T.C. contributed to study design, provided clinical and medical guidance, and supervised the study. Z.H. conceived and led the study, supervised the project, and critically revised the manuscript. All authors read and approved the final manuscript.

Acknowledgements We thank the UK Biobank participants and research team for their contributions to this resource. We also acknowledge the FinnGen study participants and investigators for making their GWAS summary statistics publicly available, and the investigators of the CMR genome-wide association studies for sharing the summary statistics used in this study.

Supplementary Information

Additional file 1: Supplementary Methods and Figures (.docx). Supplementary Methods: CMR acquisition and processing; covariate definitions and data handling; sensitivity and right-left paired analyses; antidepressant use and mental health consultation; metabolic syndrome; propensity-score matching and effect-modification analyses; PHQ-2 analyses; biomarker preprocessing; GWAS harmonization; and supporting MR analyses. Figure S1: Representative CMR traits associated with pre-imaging MDD. Figure S2: Antidepressant-class comparisons of

CMR traits within participants with MDD. Figure S3: Disease-duration-specific right-left CMR associations. Figure S4: PHQ-2 associations with paired right- and left-heart CMR traits. Figure S5: Distribution of primary mediation effects across CMR domains. Figure S6: Genetic correlations between MDD and CMR traits. Figure S7: Regional association plots for high-confidence MDD-CMR colocalized loci. Figures S8-S15: Forward, reverse and supporting MR analyses, including SNP-level and leave-one-out sensitivity analyses. Figure S16: Five-year decision-curve analysis for CVD. Figure S17: C-index across CVD endpoints. Figure S18: Risk stratification across CVD endpoints.

Additional file 2: Supplementary Tables (.xlsx). Table S1: Definitions and classification of the 82 CMR traits. Table S2: Characteristics of the study cohorts. Table S3: Primary MDD-CMR associations. Table S4: Paired right-left comparisons. Table S5: Extended covariate-adjusted and overlap-weighted sensitivity analyses. Table S6: Antidepressant class-specific analyses. Table S7: Right-left comparisons across sensitivity analyses. Table S8: Propensity-score-matched analyses within participants with MDD. Table S9: Effect-modification and stratified analyses. Table S10: Disease-duration-specific associations. Table S11: PHQ-2 associations. Table S12: Candidate biomarker associations. Table S13: Primary mediation analyses and right-left mediation comparisons. Table S14: GWAS data sources. Table S15: Genetic correlations. Table S16: High-confidence colocalized loci and functional annotation. Table S17: MR analyses and sensitivity summaries. Table S18: Overall CVD prediction. Table S19: CVD subtype prediction and contributions of individual right-heart CMR traits.

Additional file 3: Supplementary Data (.xlsx). Supplementary Data 1: Full effect-modification results. Supplementary Data 2: Full stratified-association results. Supplementary Data 3: Disease-duration restricted cubic spline results. Supplementary Data 4: Exploratory Olink mediation analyses. Supplementary Data 5: MDD genetic instruments. Supplementary Data 6: Forward MR results across methods. Supplementary Data 7: MR sensitivity analyses. Supplementary Data 8: Reverse MR results. Supplementary Data 9: SNP-level leave-one-out MR results. Supplementary Data 10: Supporting MR analyses using published CMR GWAS. Supplementary Data 11: Complete MDD-CMR colocalization scan.

References

[1] Marx, W., *et al.* Major depressive disorder. *Nature Reviews Disease Primers* **9**, 44 (2023).

[2] GBD 2019 Mental Disorders Collaborators. Global, regional, and national burden of 12

mental disorders in 204 countries and territories, 1990-2019: a systematic analysis for the Global Burden of Disease Study 2019. *Lancet Psychiatry* **9**, 137-150 (2022).

[3] Frank, P.*, et al.* Association between depression and physical conditions requiring hospitalization. *JAMA psychiatry* **80**, 690-699 (2023).

[4] Momen, N.C.*, et al.* Association between mental disorders and subsequent medical conditions. *New England Journal of Medicine* **382**, 1721-1731 (2020).

[5] Harshfield, E.L.*, et al.* Association between depressive symptoms and incident cardiovascular diseases. *Jama* **324**, 2396-2405 (2020).

[6] Pan, A., Sun, Q., Okereke, O.I., Rexrode, K.M. & Hu, F.B. Depression and risk of stroke morbidity and mortality: a meta-analysis and systematic review. *JAMA* **306**, 1241-1249 (2011).

[7] Shi, S., Liu, T., Liang, J., Hu, D. & Yang, B. Depression and Risk of Sudden Cardiac Death and Arrhythmias: A Meta-Analysis. *Psychosom Med* **79**, 153-161 (2017).

[8] Miller, A.H. & Raison, C.L. The role of inflammation in depression: from evolutionary imperative to modern treatment target. *Nat Rev Immunol* **16**, 22-34 (2016).

[9] Stetler, C. & Miller, G.E. Depression and hypothalamic-pituitary-adrenal activation: a quantitative summary of four decades of research. *Psychosom Med* **73**, 114-126 (2011).

[10] Vaccarino, V.*, et al.* Depression and coronary heart disease: 2018 position paper of the ESC working group on coronary pathophysiology and microcirculation. *Eur Heart J* **41**, 1687-1696 (2020).

[11] Colangelo, L.A.*, et al.* Association of 20-Year Longitudinal Depressive Symptoms With Left Ventricular Geometry Outcomes in the Coronary Artery Risk Development in Young Adults Study: A Role for Androgens? *Psychosom Med* **86**, 60-71 (2024).

[12] Santiago, C.*, et al.* Association between depressive symptoms and cardiac structure and function in a Peruvian population. *Global Heart* **17**, 78 (2022).

[13] Vu, K.*, et al.* Depressive Symptoms, Cardiac Structure and Function, and Risk of Incident Heart Failure With Preserved Ejection Fraction and Heart Failure With Reduced Ejection Fraction in Late Life. *J Am Heart Assoc* **10**, e020094 (2021).

[14] Gustad, L.T.*, et al.* Cardiac function associated with previous, current and repeated depression and anxiety symptoms in a healthy population: the HUNT study. *Open Heart* **3**, e000363 (2016).

[15] Alfakih, K., Reid, S., Jones, T. & Sivananthan, M. Assessment of ventricular function

and mass by cardiac magnetic resonance imaging. *European Radiology* **14**, 1813-1822 (2004).

[16] Petersen, S.E.*, et al.* UK Biobank's cardiovascular magnetic resonance protocol. *Journal of Cardiovascular Magnetic Resonance* **18**, 8 (2016).

[17] Zhao, B.*, et al.* Heart-brain connections: Phenotypic and genetic insights from magnetic resonance images. *Science* **380**, abn6598 (2023).

[18] Sudlow, C.*, et al.* UK biobank: an open access resource for identifying the causes of a wide range of complex diseases of middle and old age. *PLoS Med* **12**, e1001779 (2015).

[19] Littlejohns, T.J.*, et al.* The UK Biobank imaging enhancement of 100,000 participants: rationale, data collection, management and future directions. *Nat Commun* **11**, 2624 (2020).

[20] Benjamini, Y. & Hochberg, Y. Controlling the False Discovery Rate: A Practical and Powerful Approach to Multiple Testing. *Journal of the Royal Statistical Society: Series B (Methodological)* **57**, 289-300 (1995).

[21] Thomas, L.E., Li, F. & Pencina, M.J. Overlap Weighting: A Propensity Score Method That Mimics Attributes of a Randomized Clinical Trial. *JAMA* **323**, 2417-2418 (2020).

[22] Kroenke, K., Spitzer, R.L. & Williams, J.B. The Patient Health Questionnaire-2: validity of a two-item depression screener. *Med Care* **41**, 1284-1292 (2003).

[23] Bergstedt, J.*, et al.* Distinct biological signature and modifiable risk factors underlie the comorbidity between major depressive disorder and cardiovascular disease. *Nat Cardiovasc Res* **3**, 754-769 (2024).

[24] Penninx, B.*, et al.* Immuno-metabolic depression: from concept to implementation. *Lancet Reg Health Eur* **48**, 101166 (2025).

[25] Sun, B.B.*, et al.* Plasma proteomic associations with genetics and health in the UK Biobank. *Nature* **622**, 329-338 (2023).

[26] Tingley, D., Yamamoto, T., Hirose, K., Keele, L. & Imai, K. mediation: R Package for Causal Mediation Analysis. *Journal of Statistical Software* **59**, 1 - 38 (2014).

[27] Kurki, M.I.*, et al.* FinnGen provides genetic insights from a well-phenotyped isolated population. *Nature* **613**, 508-518 (2023).

[28] Bai, W.*, et al.* A population-based phenome-wide association study of cardiac and aortic structure and function. *Nat Med* **26**, 1654-1662 (2020).

[29] Aung, N.*, et al.* Genome-wide association analysis reveals insights into the genetic

architecture of right ventricular structure and function. *Nature Genetics* **54**, 783-791 (2022).

[30] Pirruccello, J.P.*, et al.* Analysis of cardiac magnetic resonance imaging in 36,000 individuals yields genetic insights into dilated cardiomyopathy. *Nature communications* **11**, 2254 (2020).

[31] Tadros, R.*, et al.* Large-scale genome-wide association analyses identify novel genetic loci and mechanisms in hypertrophic cardiomyopathy. *Nat Genet* **57**, 530-538 (2025).

[32] Bulik-Sullivan, B.K.*, et al.* LD Score regression distinguishes confounding from polygenicity in genome-wide association studies. *Nat Genet* **47**, 291-295 (2015).

[33] Grotzinger, A.D.*, et al.* Genomic structural equation modelling provides insights into the multivariate genetic architecture of complex traits. *Nat Hum Behav* **3**, 513-525 (2019).

[34] Ning, Z., Pawitan, Y. & Shen, X. High-definition likelihood inference of genetic correlations across human complex traits. *Nature Genetics* **52**, 859-864 (2020).

[35] Wallace, C. Eliciting priors and relaxing the single causal variant assumption in colocalisation analyses. *PLoS Genetics* **16**, e1008720 (2020).

[36] Giambartolomei, C.*, et al.* Bayesian test for colocalisation between pairs of genetic association studies using summary statistics. *PLoS genetics* **10**, e1004383 (2014).

[37] Harrow, J.*, et al.* GENCODE: the reference human genome annotation for The ENCODE Project. *Genome Res* **22**, 1760-1774 (2012).

[38] Fabregat, A.*, et al.* The Reactome Pathway Knowledgebase. *Nucleic Acids Res* **46**, D649-D655 (2018).

[39] Kanehisa, M., Furumichi, M., Sato, Y., Ishiguro-Watanabe, M. & Tanabe, M. KEGG: integrating viruses and cellular organisms. *Nucleic Acids Res* **49**, D545-D551 (2021).

[40] Raudvere, U.*, et al.* g:Profiler: a web server for functional enrichment analysis and conversions of gene lists (2019 update). *Nucleic Acids Res* **47**, W191-W198 (2019).

[41] The Gene Ontology Consortium. The Gene Ontology resource: enriching a GOld mine. *Nucleic Acids Research* **49**, D325-D334 (2021).

[42] Hemani, G.*, et al.* The MR-Base platform supports systematic causal inference across the human phenome. *eLife* **7**, e34408 (2018).

[43] The 1000 Genomes Project Consortium. A global reference for human genetic variation. *Nature* **526**, 68-74 (2015).

[44] Bowden, J., Davey Smith, G. & Burgess, S. Mendelian randomization with invalid instruments: effect estimation and bias detection through Egger regression. *International Journal of Epidemiology* **44**, 512-525 (2015).

[45] Bowden, J., Davey Smith, G., Haycock, P.C. & Burgess, S. Consistent estimation in Mendelian randomization with some invalid instruments using a weighted median estimator. *Genetic Epidemiology* **40**, 304-314 (2016).

[46] Verbanck, M., Chen, C.-Y., Neale, B. & Do, R. Detection of widespread horizontal pleiotropy in causal relationships inferred from Mendelian randomization between complex traits and diseases. *Nature Genetics* **50**, 693-698 (2018).

[47] Harrell, F.E., Lee, K.L. & Mark, D.B. Multivariable prognostic models: issues in developing models, evaluating assumptions and adequacy, and measuring and reducing errors. *Statistics in Medicine* **15**, 361-387 (1996).

[48] Royston, P. & Sauerbrei, W. A new measure of prognostic separation in survival data. *Statistics in Medicine* **23**, 723-748 (2004).

[49] Pencina, M.J., D'Agostino, R.B., Sr., D'Agostino, R.B., Jr. & Vasan, R.S. Evaluating the added predictive ability of a new marker: from area under the ROC curve to reclassification and beyond. *Stat Med* **27**, 157-172; discussion 207-112 (2008).

[50] Vickers, A.J. & Elkin, E.B. Decision curve analysis: a novel method for evaluating prediction models. *Medical Decision Making* **26**, 565-574 (2006).

[51] Bueno, H.*, et al.* 2025 ESC Clinical Consensus Statement on mental health and cardiovascular disease: developed under the auspices of the ESC Clinical Practice Guidelines Committee. *Eur Heart J* **46**, 4156-4225 (2025).

[52] Haddad, F., Hunt, S.A., Rosenthal, D.N. & Murphy, D.J. Right ventricular function in cardiovascular disease, part I: Anatomy, physiology, aging, and functional assessment of the right ventricle. *Circulation* **117**, 1436-1448 (2008).

[53] Tello, K., Naeije, R., de Man, F. & Guazzi, M. Pathophysiology of the right ventricle in health and disease: an update. *Cardiovasc Res* **119**, 1891-1904 (2023).

[54] Hahn, R.T.*, et al.* Multimodality Imaging of Right Heart Function: JACC Scientific Statement. *J Am Coll Cardiol* **81**, 1954-1973 (2023).

[55] Hemnes, A.R.*, et al.* Pathophysiology of the right ventricle and its pulmonary vascular interaction. *Eur Respir J* **64**, 2401321 (2024).

[56] Kemp, A.H.*, et al.* Impact of depression and antidepressant treatment on heart rate

variability: a review and meta-analysis. *Biol Psychiatry* **67**, 1067-1074 (2010).

[57] Nemeroff, C.B. & Goldschmidt-Clermont, P.J. Heartache and heartbreak--the link between depression and cardiovascular disease. *Nat Rev Cardiol* **9**, 526-539 (2012).

[58] Caporizzo, M.A. & Prosser, B.L. The microtubule cytoskeleton in cardiac mechanics and heart failure. *Nat Rev Cardiol* **19**, 364-378 (2022).

[59] Robison, P.*, et al.* Detyrosinated microtubules buckle and bear load in contracting cardiomyocytes. *Science* **352**, aaf0659 (2016).

[60] Chen, C.Y.*, et al.* Suppression of detyrosinated microtubules improves cardiomyocyte function in human heart failure. *Nat Med* **24**, 1225-1233 (2018).

[61] Kim, Y.G.*, et al.* Association of Depression With Atrial Fibrillation in South Korean Adults. *JAMA Netw Open* **5**, e2141772 (2022).

[62] Wu, F.*, et al.* Knowledge-Empowered, Collaborative, and Co-Evolving AI Models: The Post-LLM Roadmap. *Engineering* **44**, 87-100 (2025).

[63] Xu, J.*, et al.* Foundations and Applications of Information Systems Dynamics. *Engineering* **27**, 254-265 (2023).

[64] Ghorbankhani, M. & Safara, M. Artificial intelligence in depression diagnostics: A systematic review of methodologies and clinical applications. *Artif Intell Med* **172**, 103320 (2026).

[65] Moumgiakmas, S.S., Vrochidou, E. & Papakostas, G.A. Mapping the brain: AI-driven radiomic approaches to mental disorders. *Artif Intell Med* **168**, 103219 (2025).

[66] Sun, K.*, et al.* Medical multimodal foundation models in clinical diagnosis and treatment: Applications, challenges, and future directions. *Artif Intell Med* **170**, 103265 (2025).

[67] Schoeler, T.*, et al.* Participation bias in the UK Biobank distorts genetic associations and downstream analyses. *Nat Hum Behav* **7**, 1216-1227 (2023).

Supplementary Files

This is a list of supplementary files associated with this preprint. Click to download.

- SupplementaryTables1026.xlsx
- SupplementaryInformation1013.docx
- SupplementaryData1008.xlsx